# Effects of Lateral Confinement on Order in Spherical Domain Block Copolymer Thin Films

**Rachel A. Segalman, Alexander Hexemer, and Edward J. Kramer***

*Departments of Chemical Engineering and Materials, University of California, Santa Barbara, Santa Barbara, California 93106*

*Received October 23, 2002*

ABSTRACT: A topographically patterned substrate can be used to template a large, single crystalline grain of block copolymer spherical domains. Both the geometry of the substrate and the annealing temperature can be used to control the degree of order as well as the crystallographic orientation of the grain. The presence of a hard edge imparts translational order onto the hexatic, which has quasi-long-range orientational order and short-range translational order, and onto the liquid which has short-ranged translational and orientational order. This ordering influence is seen to fade as the distance from the edge increases. As a result, the regions near the edge appear to melt from crystalline order to hexatic by dislocation pair unbinding and then to a liquid through a disclination unbinding transition at higher temperatures than regions far from the edges. Crystalline grains templated by a hard step wall also have superior translational order as compared to those templated by a vacuum edge. The adjacent step also plays a crucial role in determining the grain orientation of the crystalline array on top of a mesa.

## Introduction

Diblock copolymers have been used to pattern features on the nanometer scale for semiconductor and magnetic storage applications[1−4] and have served as sites for the inorganic synthesis of a variety of metallic dots[5,6] and nanowires.[7,8] The application of these materials to patterning requires precise control over the orientation and registry of a single layer of the nanometer sized domain structures over large areas. Domain orientation in cylinder and lamella forming diblock copolymers has been successfully controlled by using external fields such as electrical fields[9,10] and surface interactions.[11−14] Graphoepitaxy has also been used to achieve long-range order of spherical domains via topographical templating.[15] This use of substrate patterning to control domain order resulted in a single layer of block copolymer spheres arranged into a two-dimensional, hexagonally packed crystal at least 4.5 $\mu$m in width. It has been proposed by Trawick et al. that after very short annealing times (at temperatures above the glass transition temperature of the system) small grains of the hexagonal 2D structure nucleate randomly on the surface. There soon appears to be a dominant grain orientation near the edges of the substrate topography. This long, narrow single-crystal now grows as its grain boundary sweeps across the fine grained polycrystalline array further away from the edge.[16]

While attempts to control the orientation of the block copolymer microdomains have focused on controlling interfacial interactions, there is also a recognized need to balance the kinetic limitations of polymer diffusion with the thermodynamics of microphase segregation to optimize long-range order. Experiments,[17−23] computer simulations,[24] and theoretical developments[25,26] have led to a better understanding of how a bulk sample of asymmetric copolymer, which forms spherical micelles ordered on a body-centered-cubic (bcc) lattice at large $\chi N_{min}$ (where $\chi$ is the temperature-dependent Flory Huggins parameter and $N_{min}$ is the length of the smaller of the two blocks) disorders as $\chi N_{min}$ is decreased. There is also evidence to suggest that the ordering process in a thin film is not analogous to that in bulk. For instance, the presence of substrate surfaces has been shown in both experiments[27−32] and simulations [33,34] to induce layering in thick films of poorly ordered and disordered block copolymers. In the truly 2-D case of a single layer of block copolymer spheres, the melting transition is fundamentally different in both absolute temperature and qualitative character than the 3-D lattice disordering transition observed in bulk samples.[35] In particular, a 3-D solid has long-range translational and orientational order. By contrast, the long-range translational order of a 2-D crystal is destroyed by thermally excited long wavelength phonons so that it has only quasi-long-range translational order.[36−39] Despite the decrease in translational order, however, long-range orientational order is present in the 2-D solid.[40]

The effectiveness of graphoepitaxy on ordering a system consisting of only one layer of block copolymer spheres is very dependent on the temperature of annealing. In particular, at high values of $\chi N_{min}$ graphoepitaxy is not an efficient means for removing grain boundaries since the system does not have enough mobility. At low values of $\chi N_{min}$, dislocation-mediated melting following the theoretical sequence predicted by the papers of Kosterlitz, Thouless, Halperin, Nelson, and Young (KTHNY theory)[41−45] is observed. In 2-D crystals, an equilibrium number of dislocations, usually in pairs with opposite Burgers vectors, will exist at any temperature. Since this equilibrium number of dislocations will increase with temperature, there is an optimum temperature at which graphoepitaxy will form a single grain with a minimum number of defects.

Halperin and Nelson predict that the continuous melting transition from a 2-D crystal to a liquid will proceed through a hexatic intermediate phase that will possess short-range translational order but quasi-long-range orientational order.[43,44] The 2-D hexatic−isotropic liquid transition of a layer of block copolymer spheres near a hard edge on the substrate was observed to occur at a lower temperature (~30 K lower) than the 3-D lattice disordering temperature.[35] Surface effects in 3-D

10.1021/ma0257696 CCC: $25.00 
Published on Web 08/09/2003

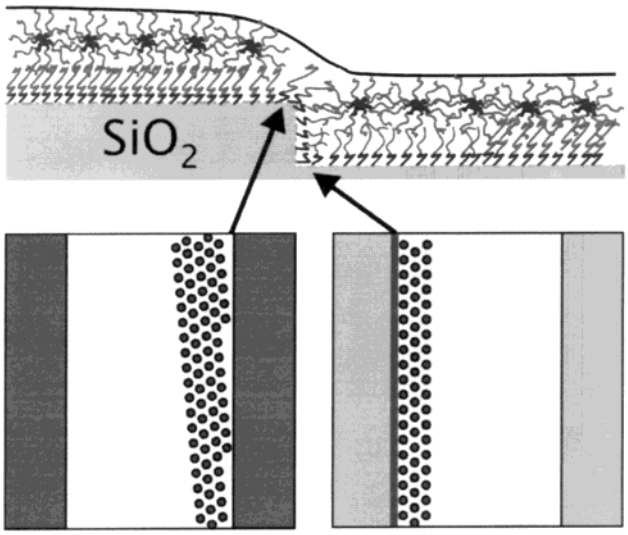


**Figure 1.** Schematic of a layer of block copolymer at a mesa−well edge interface on a patterned substrate. The silicon oxide surface is coated by a PS−PVP brush and a single layer of spheres.

have been demonstrated to have an ordering influence on block copolymer systems.[27−31,33,34] It is therefore likely that the edges of the patterned substrate in a 2-D block copolymer film influence not only whether the surrounding array is polycrystalline or not, but also the translational and orientational order within the block copolymer domain array near such edges. One consequence would be that the 2-D hexatic to isotropic liquid transition should be a function of distance from a hard edge, a feature verified in a recent communication.[46]

In this paper, the effects of substrate topography and annealing temperature on graphoepitaxy will be presented. An alternating series of raised mesas with wells between them on the substrate served to provide lateral surfaces from which graphoepitaxy can occur. In particular, the hard edge of the well (depicted schematically in Figure 1) templates much better order than does the deformable edge of the mesa. The two-stage melting of block copolymer spheres in 2-D is also affected by the presence of substrate topography. In particular, the presence of a hard edge imparts additional orientational order to the hexatic phase and suppresses melting via disclination unbinding in its vicinity. We will also discuss how the geometry of the substrate affects the grain orientation of the crystal. In particular, the curvature of the edges of mesas, caused by surface area minimization, causes a reorientation of the crystalline array.

## Experimental Section

Polystyrene-*b*-(2-vinylpyridine) (PS−PVP) was synthesized via anionic polymerization as previously documented[32] with $N = 670$ and $f_{PVP} = 0.129$, where $N$ is the total degree of polymerization of the block copolymer and $f_{PVP}$ is the mole fraction of PVP mers. This material self-assembles in the bulk to form spherical PVP cores 9 nm in diameter surrounded by PS coronae arranged in bcc arrays with a (110) plane spacing of 27 nm.

Silicon substrates were obtained from Cypress Semiconductor Corp. (Minneapolis, MN), and layers of silicon oxide of thickness 15 nm $\leq h \leq$ 300 nm were deposited on the wafers by electron beam evaporation. The substrate was then patterned with a series of mesas and wells via standard photolithography and chemical etching with hydrofluoric acid. A 1.5 nm thick native oxide layer was then allowed to regrow on all etched surfaces. The resulting raised mesas and depressed wells were up to 1 mm long and 15 $\mu$m wide with a height difference between mesa and well of $h$.

PS−PVP films were spun-cast from dilute (∼1%) toluene solution directly onto the patterned substrates when the mesa height was less than 50 nm. The film thickness was held at ∼50 nm by varying the spin speed and concentration. For taller mesas ($h$ > 50 nm), meniscus buildup of material near the edges of the wells is more noticeable, and it is difficult to cast a film of uniform thickness. In these cases, uniform films were first cast onto small sections of glass microscope slides (1 cm$^2$) and then slowly released from the slide onto the surface of a distilled water bath. The floating film was then retrieved onto the patterned substrate.

All samples were annealed at a designated temperature in high vacuum (<$10^{-6}$ Torr) for 72 h to allow ordering. The samples were then quenched to below the glass transition temperature (∼100 °C) to lock in the structure. This resulted in a 20 nm PS−PVP brush at the silicon surface followed by a layer of PVP cores surrounded by PS corona matrix as previously documented.[15,35] The substrate topography was visible via optical microscopy and scanning force microscopy (SFM), but the film was smooth on a 5 nm scale and the presence of the PVP cores was not obvious.

The oxygen ion gun of a Physical Electronics 6650 dynamic secondary ion mass spectrometer (SIMS) was used to etch to the midplane of the layer of PVP spheres. The 1 kV beam of $O_2^+$ ions was rastered over a 0.09 mm$^2$ crater to etch the material while a static, defocused 1 keV electron beam was centered on the crater to neutralize the charge. Negative ions of H, CN, and Si were monitored as a function of time. The etch was halted at a local maximum in the $CN^-$ signal that indicated the location of the midplane of a layer of spheres. The polar PVP cores were etched slightly faster than the surrounding PS matrix resulting a 1 nm deep dimple in the center of every sphere. Tapping mode scanning force microscopy (SFM) performed on a Digital Instruments MultiMode AFM was used to detect the placement of the PVP cores (dimples). Image processing and sphere center detection were performed as previously described.[35]

## Results and Discussion

Steps in the substrate topography can align the spherical microdomains of an asymmetric diblock copolymer film. The spheres are arranged in hexagonal arrays within a few micrometers of the templating edge. The crystallographic orientation of the resulting hexagonal grain can be controlled by both the geometry of the confining surfaces and the temperatures at which the system is annealed. Similarly, the perfection of this grain and the melting transition are also controlled by an interplay of substrate geometry and annealing temperature.

**Control of Crystallographic Orientation.** Islands and holes form in a thin film of this asymmetric PS−PVP diblock copolymer when the original, spun-cast film thickness does not match a natural thickness, $h$, given approximately by

$$h = \alpha n + \beta \qquad (1)$$

where $\alpha$ is the thickness of a layer of spheres (27 nm at 180 °C), $\beta$ is the thickness of a layer of PS−PVP brush adsorbed on the silicon oxide surface (20 nm at 180 °C), and $n$ is an integer value.

In previous studies, attention was focused on surfaces patterned with mesa topographies of height $\alpha$ so that the raised mesas resembled naturally occurring islands. This arbitrary height was chosen since graphoepitaxy of inorganic material usually requires a surface relief structure that is at least one molecular unit high.[47]

Changing the height of the mesas (and consequently the depth of the wells) may change the interfacial energy of the material at the mesa edge. As a result, the crystallographic orientation of the close-packed rows in the hexagonal structure may vary simply to reduce the interfacial energy.

Surface relief structures less than one sphere unit high, 3−15 nm (0.1α−0.5α), have no templating effect. Grain boundaries occur around and through each of these patterns. Mesas α high (and wells α deep) template single crystalline arrays of hexagonally packed spheres when annealed at 180 °C for 72 h at high vacuum.[15]

In the well, the spheres align with the hard silicon oxide step edge which is coated with a PS−PVP brush, as schematically depicted in Figure 1. In this region, the spheres are oriented with a close-packed direction parallel to the step edge so that a maximum number of spheres are in close proximity to the PS−PVP brush. On the mesa, the spheres are templated by the vacuum edge shown in Figure 1. The surface energy of the polymer film at the mesa edge forces the step edge of the polymer surface to be curved and compresses the spheres closest to the edge. When the mesa is α high, the polymer surface curvature is rather sharp as shown in Figure 2. In this geometry, an angle of approximately 5° between the close-packed line of spheres and the step edge is observed. The mesa can template two grain orientations with respect to its edge, +5° and −5° orientations, raising the likelihood of grain boundaries in the block copolymer array on the mesa. It is possible that this low-angle grain boundary may migrate by the glide of its component dislocations to one side of the mesa or the other during the annealing process, resulting in high-quality, single crystalline arrays. SFM images, such as the 1.5 $\mu$m square images shown in Figure 2, depict the arrangement of the PVP cores as dark regions (depressions). In Figure 2b, a confining mesa edge is to the right of the image, and the close-packed rows extend away from the wall at an angle of 5°. This single grain can span widths as broad as 4.5 $\mu$m, running along the entire length of each mesa.The crystals in the wells are equally large, but these are oriented so that a close-packed row is parallel to the edge.

Voronoi constructions[48] displayed above the associated Fourier transforms of the 2-D array of sphere centers aid in the recognition of point defects such as dislocations and disclinations. This diagram is created by drawing bonds to connect the center of each sphere to its neighbors. The perpendicular bisectors of these bonds intersect to form a polygon. The polygon has a number of sides equal to the number of nearest neighbors of the sphere in the center. The 6-fold-coordinated sites appear as hexagons while 5's are displayed as pentagons and 7's are displayed as heptagons. The 5's represent points at which a 60° wedge has been removed and are therefore actually −60° disclinations. The 7's, correspondingly, are +60° disclinations. A dislocation core is seen as a bound 5−7 pair, and a grain boundary is seen as a row of dislocations. The Voronoi diagram in the middle row of Figure 2b demonstrates that in this 1.5 $\mu$m square area no grain boundaries are present and only one dislocation is visible. The associated Fourier transform at the bottom of Figure 2b confirms the fact that the area is single crystalline.

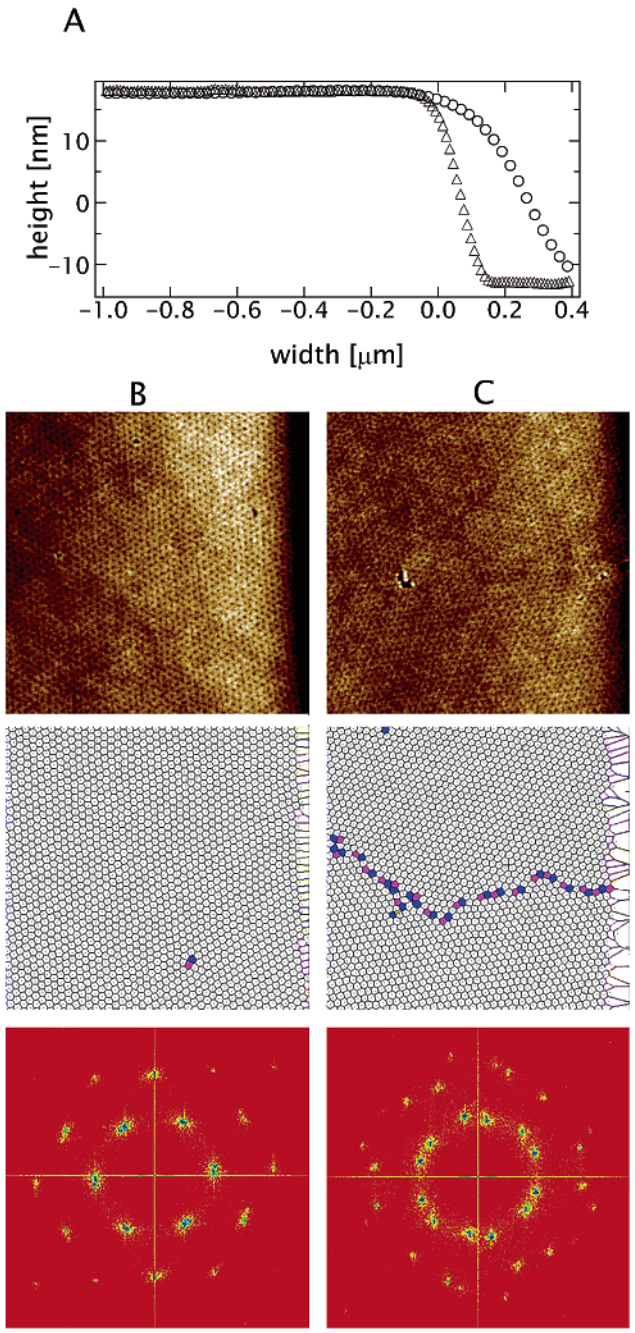


**Figure 2.** Spherical domains of block copolymers on mesas. (A) A line scan from SFM of the mesa edge on top of a 30 nm high step (△) and a 300 nm high step (○). 1.5 $\mu$m square SFM images of etched arrays of spheres on the mesa edges of a (B) 30 nm step and (C) a 300 nm step (vacuum edges are to the right of each image) with a 5 nm height scale (from dark to bright). The PVP cores appear as 1 nm dimples (dark) in the higher matrix. The middle panels are Voronoi diagrams constructed from the sphere center locations. The 6-fold coordinated sites are unshaded while 5-fold sites are magenta and 7-fold sites are blue. The bottom panels are Fourier transforms with false color (low scattering intensities are shaded red and high intensities are blue). Near the 300 nm high step, a 20° grain boundary is present running perpendicular to the step edge.

The templating effect of the well is strong enough that if the geometry of the well is changed so that the edges no longer run parallel to each other, a grain boundary can be templated. Each edge nucleates a grain with the close-packed row oriented parallel to the edge. When the two grains meet in the middle of the angular well,

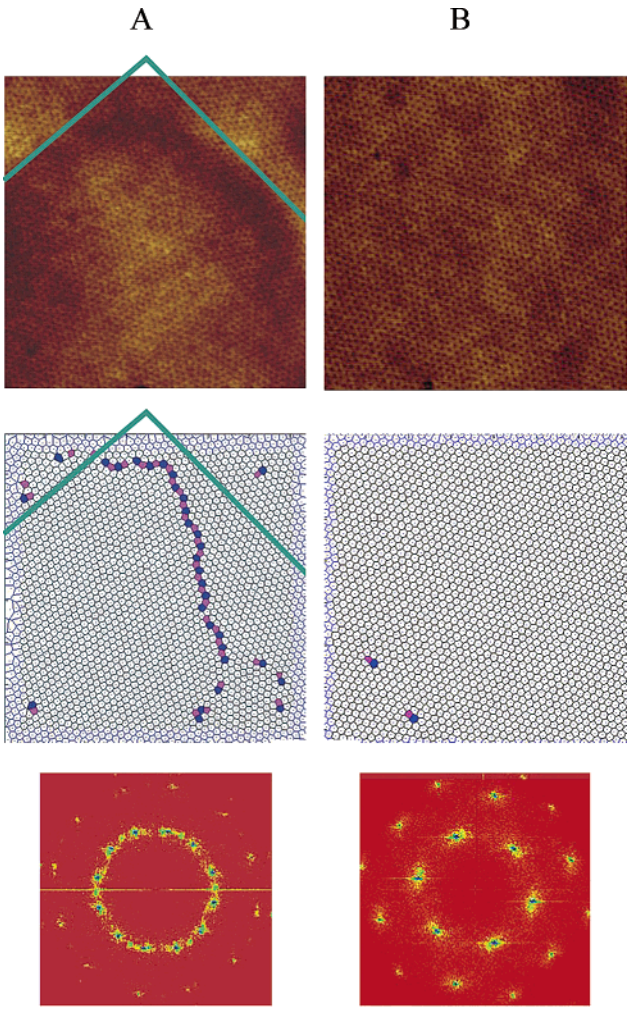


**Figure 3.** The 1.5 $\mu$m square SFM images, Voronoi constructions, and Fourier transforms of arrays of spheres confined in (A) a 90° corner of a well (substrate edges are drawn in blue). In a triangular well where the walls are at 60° angles, a single grain exists within the center of the well (B).

there is a grain misorientation unless the angle between the edges of the well is 0° modulo 60°. Figure 3a includes the 1.5 $\mu$m square SFM image, associated Voronoi construction, and Fourier transforms from the 90° corner of a well where each side has templated a different grain orientation. These two grains meet to form a 30° grain boundary in the middle of the corner. This angle happens to be the largest possible for a hexagonal lattice, but shallower grain boundaries can be formed in sharper corners. In many of these cases, however, the formation of sharp corners is limited by the tendency of photolithographically patterned and chemically etched substrates to round sharp angles. Figure 3b demonstrates that when the edges of the well make a 60° angle (matching the close-packed row arrangement of the hexagonal structure), a single grain is templated, as expected, except at the rounded tip of the corner where a grain boundary occurs.

When the mesa height (for a stripe with parallel edges) is increased to 150 nm (approximately 5$\alpha$) and the film thickness and annealing temperature are still $\alpha$ and 180 °C, respectively, the curvature at the mesa boundary is much smaller. This may simply be a result of meniscus filling of the edge of the well. The close-packed row now makes an angle of ~20° with the mesa edge. In this configuration, two epitaxial orientations

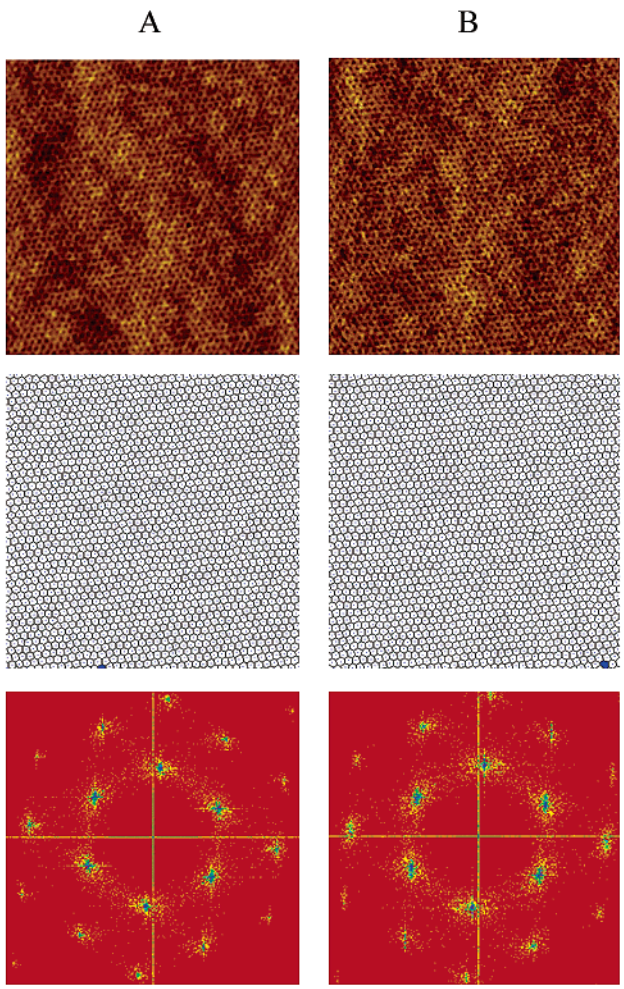


**Figure 4.** SFM micrographs, Voronoi constructions, and Fourier transforms of 1.5 $\mu$m square regions annealed at 235 °C for 72 h (a) near the edge of the well (step is to the left of the image) and (b) in the center of the 15 $\mu$m wide well.

are possible along the mesa step, +20° and −20°, which can lead to high angle grain boundaries with a total misorientation angle of 20° as seen in the 1.5 $\mu$m square SFM image in Figure 2c. These grain boundaries are roughly perpendicular to the mesa edge and occur at intervals of approximately 3 $\mu$m along the length of the mesa.

At 180 °C, graphoepitaxy can suppress grain boundaries within a 2.5 $\mu$m wide stripe near the confining edge after a 72 h anneal. At higher temperatures, the diffusion in the system is much faster, and as a result, grain boundaries can be eliminated further away from the confining edge. Within the range 235 °C $\leq T \leq$ 250 °C, a single grain spanned the entire 15 $\mu$m width of the widest well on our substrate. Figure 4 shows SFM images, Voronoi diagrams, and Fourier transforms of regions near the edge and in the middle of a well of a sample annealed at 235 °C.

When the temperature of the system is within the range 220 °C $< T \leq$ 250 °C, graphoepitaxy still produces a single crystalline grain near the edge,[35] but the orientation of the templated grain changes. The close-packed rows of spheres are arranged approximately 5° off-normal to the confining edges both on the mesa and in the well. Both the parallel and off-normal orientations appear to be an equilibrium structure and are in fact kinetically accessible regardless of the thermal history of the array. When a sample is first annealed at 235 °C

for 72 h and then at 180 °C for 72 h, the orientation of the close-packed rows appears to return to a roughly parallel arrangement with respect to the confining edge, and we find a single crystal. When the reverse thermal path is taken and the sample is first annealed at 180 °C for 72 h and then at 235 °C for 72 h, we find a mixed orientation of grains 5° and −5° off-normal to the edge. The grain boundary created has a misorientation angle of 10° and is oriented roughly normal to the edge of the well. The processes necessary to reorient the array from the 5° off-normal crystal to the parallel single crystal in this thermal cycle have to be quite different from those proposed as explaining the initial growth of the single crystal during graphoepitaxy.[16]

**Confinement Effects on Long-Range Order in the Crystal.** Given that the mesas and wells can impart different crystallographic orientations, it is natural to suspect that the quality of the order templated by these two surfaces is different. Unlike its 3-D analogue, the 2-D crystal will contain an equilibrium number of dislocations which are point defects in two dimensions. A dislocation pair consisting of two 5-fold symmetric sites (5's) and two 7-fold symmetric sites (7's) can be created or annihilated without the movement of a large amount of material (core centers). These two dislocations can then glide or climb apart (unbind), creating a disruption in the translational order of the system. There is a large energy required to separate the pair in the absence of other dislocations to screen the strain field. The energy of each dislocation is proportional to log($r$), where $r$ is the distance between a pair of dislocations with opposite Burgers vector. Therefore, once a pair of dislocations is separated, it is easier to separate (unbind) other pairs in the vicinity. Dislocations occur only infrequently in the crystalline arrays of block copolymer spheres at equilibrium (at 235 °C the dislocation density is much less than $1/\mu m^2$).[35] Because of the autocatalytic nature of the dislocation pair unbinding process, however, dislocations occur with rapidly increasing frequency at higher temperatures until the temperature is reached at which the mechanical stability of the array is compromised. The dislocation pair unbinding transition leads to a continuous transition to a hexatic array. As temperature is raised further, the dislocations themselves unbind into disclinations (isolated 5's and 7's). These individual disclinations disrupt the hexagonal nature of the array (orientational order) and lead to the Halperin−Nelson (H−N) hexatic to liquid-phase transition.

A dislocation in two dimensions consists of a bound 5−7 pair that occurs at the intersection of the two extra half lines of material (dislocation core). The energy of an isolated disclination (+60° or −60°) is proportional to the square of the distance to the nearest disclination of opposite sign. For this reason, it is not surprising that isolated disclinations are not observed until the system is almost completely melted, and in general 5's and 7's are observed in nearly identical numbers.

The degree of local order can be quantified by counting disclinations, but this count does not take into account the bound or isolated state of the defects and therefore is not useful in pinpointing the disclination unbinding transition. In Figure 5, the fraction of 5's (equal to the fraction of 7's) observed at the edge of the well and mesa are plotted as a function of temperature. The nature of the edge (the vacuum edge of the mesa as compared to hard wall of the well) does not seem to affect the number density of defects, as the defect counts on the mesa and in the well are very similar.

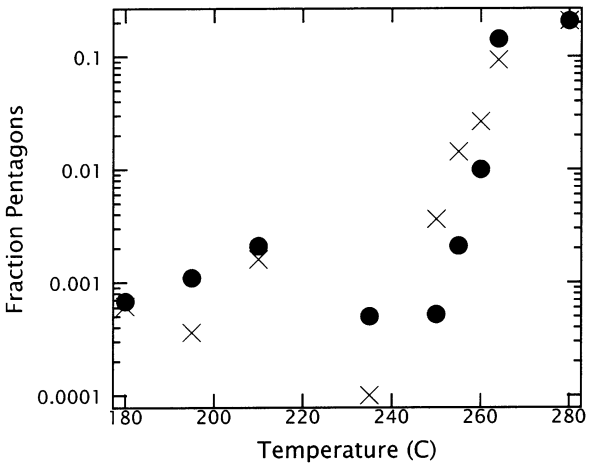


**Figure 5.** Average defect densities in the well (×) and on the mesas (●) as a function of temperature. The fraction of total Voronoi polygons that are pentagons (−60° disclinations (shown)) is equal to the fraction of heptagons (+60° disclinations, not shown). The fraction of pentagons does not appear to be depend strongly on the substrate topography.

Whether the array is crystalline, hexatic, or liquid in two dimensions can be decided on the basis of the nature of order over long length scales. The translational order of the system is quantified by a translational correlation function, $G_T(r)$. $G_T(r)$, as defined in the following manner, allows us to measure the translational order out to the edges of each 1.5 $\mu$m square area in the SFM image. $G_T(r)$ is calculated from the measured sphere center positions using $\exp(i\vec{K}\cdot\vec{r})$ as the order parameter:

$$G_T(r) = \langle e^{i\vec{K}\cdot\vec{r}'} e^{-(i\vec{K}\cdot(\vec{r}'-\vec{r}))} \rangle \quad (2)$$

where $\vec{K}$ is a reciprocal lattice vector to one of the first-order peaks in the 2-D Fourier transform and the brackets indicate an average over all spheres separated by $\vec{r}$ and an average over all six reciprocal lattice vectors. Each pair of spheres separated by $\vec{r}$ will contribute a factor of $0 \geq {}^1/_6\sum_{i=1}^{6} e^{i\vec{K}_i\cdot\vec{r}'} e^{-(i\vec{K}_i\cdot(\vec{r}'-\vec{r}))} \geq 1$ to $G_T(r)$. Similarly, the orientational correlation function is defined as

$$G_6(r) = \langle \psi_6^*(0)\, \psi_6(r) \rangle \quad (3)$$

where

$$\psi_6(r_i) = \frac{\sum_{j=1}^{NN} \exp(6i\theta(r_{ij}))}{NN} \quad (4)$$

and $\psi_6^*(0)$ indicates the complex conjugate of the order parameter of the sphere with NN nearest neighbors which is designated as the origin. Each sphere is used as the origin for one calculation, and the angular brackets indicate an average over all spheres a distance $r$ apart. $G_6(r)$ has a value between 0 and 1 for all $r$.

The two-dimensional crystal will have quasi-long-range translational order due to its susceptibility to disordering by long wavelength phonons, so $G_T(r)$ will decay to 0 algebraically.[36−39] The orientational order will not be affected and will be long range (decaying mini-

**Table 1. Expected Order of Each Phase**

| type of order | crystal | hexatic | liquid |
|---|---|---|---|
| translational order | quasi-long range: $G_T(r) \propto (r/a)^{-\eta_T}$ | short range: $G_T(r) \propto \exp(-r/\xi_T)$ | short range: $G_T(r) \propto \exp(-r/\xi_T)$ |
| orientational order | long range: no decay | quasi-long range: $G_6(r) \propto (r/a)^{-\eta_\theta}$ | short range: $G_6(r) \propto \exp(-r/\xi_6)$ |

mally with $r$). The presence of an increasing number of dislocations in the hexatic phase destroys the quasi-long-range translational order so now $G_T(r)$ decays exponentially. While the orientational order is still quasi-long range in the hexatic, it is destroyed by the dislocation−disclination unbinding transition (H−N transition) to a liquid. The order expected for each of these phases and its effects on $G_T(r)$ and $G_6(r)$ are summarized in Table 1.

For the purposes of comparing mesa edges to well edges, it is desirable to calculate translational and orientational correlation lengths. When the order is short-range and the respective correlation function decays exponentially, it is simple to determine a correlation length by fitting the data to

$$G(r) \propto \exp\left(-\frac{r}{\xi}\right) \tag{5}$$

where $\xi$ is the correlation length. Halperin and Nelson predict that the algebraic decay characteristic of quasi-long-range translational order, $G_T(r) \sim r^{-\eta_T}$, should fall within the range of $0.25 \leq \eta_T \leq 0.33$ for a 2-D crystal. While this is generally true of our crystals, at $r > 15a$, we observe that the decay of $G_T(r)$ with $r$ is somewhat faster than algebraic. Fitting with an exponential, eq 5, however, seems to yield a reasonable estimate of the correlation length for the crystals as well as hexatics and liquids.

While the translational orders in the well and mesa, presented in Figure 6a, are comparable at the very low temperatures 180−220 °C, as the temperature is increased, the order in the well becomes far superior to that on the mesa. In the well, the confining edge is not deformable and does not allow for much fluctuation in the placement of spheres along its face. As a result, this hard edge templates a hexagonal array with good order. On the mesa, the templating surface is a vacuum edge.

As was discussed previously, when the film is slightly thicker than $h$, the natural thickness, islands form containing the excess spheres. These islands accumulate near the hard edge of the well, effectively decreasing the width of the well without adding any additional edge length. When the thickness of the original spun-cast film is slightly less than $h$, holes form in the single layer of spheres, revealing the underlying brush. As this hole structure coarsens, material is transported from the mesa to the fill the well. When $h$ is only slightly less than the natural thickness (underfilling), this results after long times of annealing in the shrinkage of the layer of spheres from the edges of the mesa so only a PS−PVP brush remains there, but the well is completely filled with a layer of spheres. The kinetics of this island/hole formation and further details on the structure of the islands and holes will be presented elsewhere.[49] For the purposes of this work, care was taken to cast films that contained slightly less than one layer of spheres, i.e., to underfill.

It is convenient to view the single layer of spheres on the mesa as a long, narrow island of material. Line tension drives the island to have relatively straight lateral edges (along the step), but these edges can still fluctuate on a micron scale. These fluctuations correspond to capillary waves for a 3-D liquid or surface roughening for a 3-D solid. This relatively straight edge templates a single grain orientation, but it is not so rigid as the hard wall and the translational order is not as long range. The topography effect is more apparent in the high-temperature limit of the crystalline phase (220−250 °C) where there is a higher degree of translational order. At temperatures higher than 250 °C, the dislocation pair creation and unbinding becomes more prevalent and the translational correlation length decreases rapidly.

The epitaxial effects of both the edges of the mesa and the well lead to long-range orientational order through most of the temperature range studied. The fit obtained using eq 5 for the orientational correlation function is rather poor when the orientational order is long-range

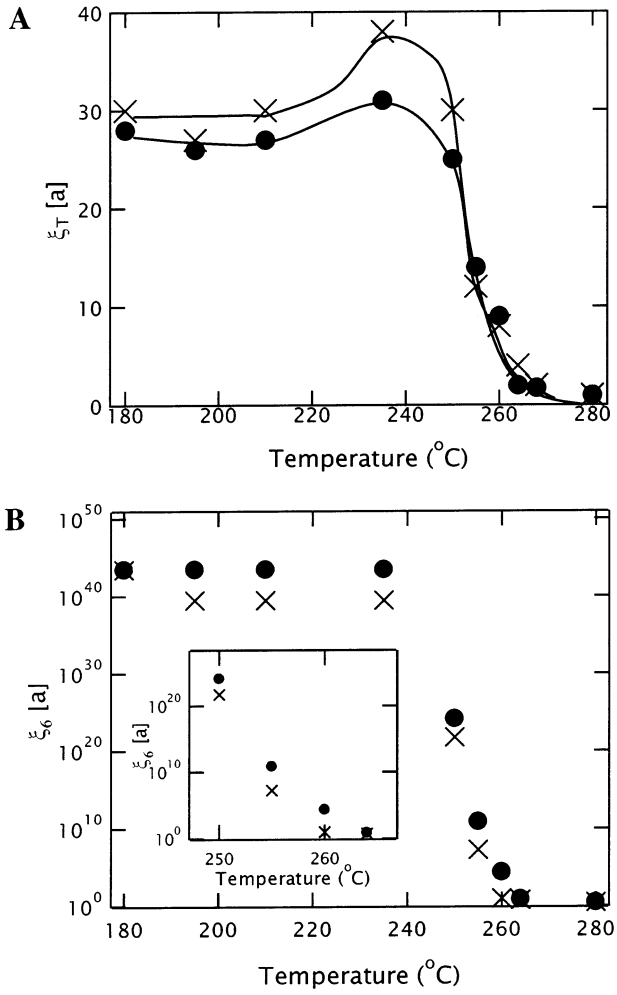


**Figure 6.** (A) Dependence of the translational correlation length on temperature near the edge of a well (×) and near the edge of a mesa (●). The hard well edge templates longer range translational order in the crystalline array than does the deformable mesa edge. (B) Dependence of orientational correlation length on temperature near the edge of a well (×) and near the edge of a mesa (●). The character of the confining surface has a less noticeable effect on the orientational order, but the mesa appears slightly better ordered than the well.

or quasi-long-range. The decay is algebraic so an approximate value for correlation length is obtained by first fitting our data with

$$G_6(r) \propto \left(\frac{r}{a}\right)^{-\eta_\theta} \tag{6}$$

where $\eta_\theta$ is the orientational order exponent. In this range we define the correlation length to be the distance beyond which $G_6(r)$ falls to below 1/e. This definition yields

$$\xi_6 = e^{1/\eta_\theta} a \tag{7}$$

The correlation lengths calculated in this manner (Figure 6b) are extremely long range (up to $10^{42}a$) in the crystalline phase and drop abruptly at the disclination unbinding transition. (This temperature range is shown as the inset in Figure 6b.) There appears to be a somewhat smaller improvement in the orientational order of the mesa over the well edge.

The well topography imparts better translational order to the block copolymer crystal than does the mesa edge, but the edge of the mesa imparts slightly better orientational order than the edge of the well. Despite the superior translational order in the well, the dislocation pair unbinding transition appears to occur at nearly the same temperature both near the edge of the mesa and near the edge of the well (as indicated by solid lines in Figure 6).

**Confinement Effects on Melting.** As the presence of substrate topography promotes the formation of single crystalline arrays, it also imparts additional orientational and translational order to the hexatic.[46] The presence of the hard well edge stabilizes the hexatic phase against the disclination unbinding transition ($T_i$) to an isotropic liquid. By stabilizing the ordered phase, the edge changes the location of the melting transition of the block copolymer system.

Figure 4 shows a representative array annealed for 72 h at 235 °C in a 15 $\mu$m wide well. Both the SFM image at the edge of the well (A) and the one in the middle of the well (B) have only one dislocation visible in the associated Voronoi construction (containing 2100 spheres each). In the crystalline regime, the density of dislocations is typically no higher away from the edge than near it. The Fourier transforms of the two regions have nearly identical orientations, suggesting that these two areas are pieces of the same very large single crystal.

Once the dislocation pair unbinding transition occurs to form the hexatic, however, the confinement produced by the edge has a more obvious effect on the local ordering. The orientational order of the hexatic is stabilized by the edge of the well, and a continuous disclination unbinding transition occurs as the distance from the edge increases.[46]

At temperatures above the disclination unbinding transition, however, the wall appears to have an ordering effect on the liquid state as well. Figure 7 depicts an array annealed for 72 h at 264 °C on a 15 $\mu$m wide well. This temperature is beyond the disclination unbinding transition both at the edge of the well and away from it, and there are quite a few free disclinations in both Voronoi diagrams. While cursory inspection of the SFM image and the associated Voronoi construction would lead one to believe that the edge of the well and the middle are very similar in terms of degree of order,

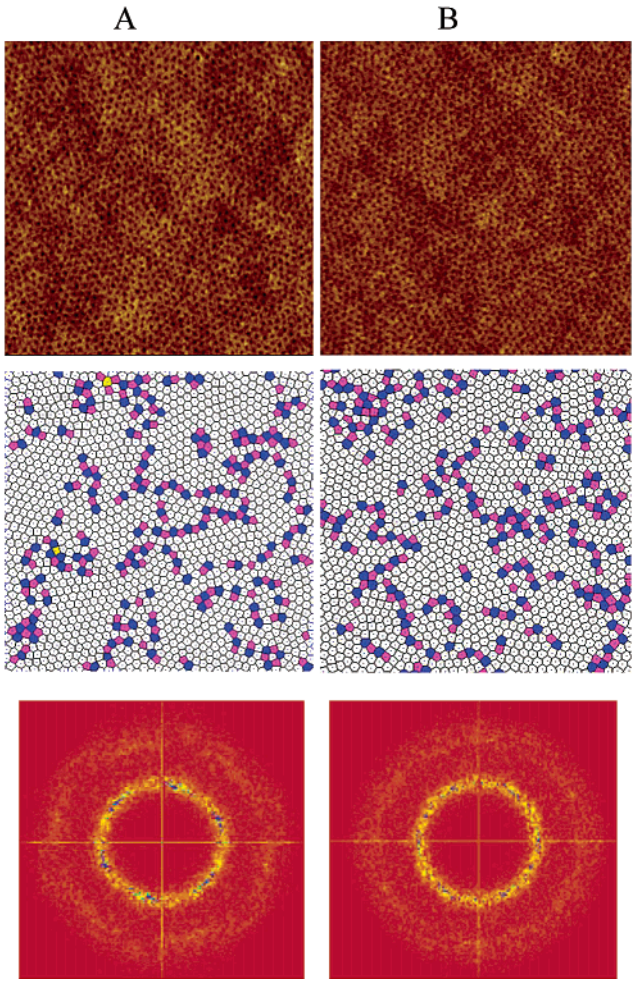


**Figure 7.** The 1.5 $\mu$m square regions annealed at 264 °C for 72 h (A) near the edge of the well (step is to the left of the image) and (B) in the center of the 15 $\mu$m wide well. The top SFM micrographs and middle Voronoi constructions seem to indicate that the two regions are similar. The Fourier transform (bottom panel) of (A), however, still shows some hexagonal symmetry while that of (B) is completely isotropic.

the Fourier transform reveals that there is 6-fold symmetry still present at the edge that is lacking in the middle of the well. In the disordered state, the wall imparts some orientational order onto the liquid.

To quantify the effects of this edge, we compare local order (by counting pentagons in the Voronoi diagrams) and translational correlation lengths, calculated as discussed previously, at the edge and in the middle of a 15 $\mu$m wide well as a function of temperature in Figure 8. The number of pentagons always seems to be higher near the center of the well than near the edge. The translational correlation lengths at the well edge and middle are also quite similar for the lower temperature crystals (180−220 °C). There is, however, an unusually high degree of translational order imparted by the hard edge of the well at 235 °C. In the middle of the well, the order at 235 °C is quite similar to that seen at the lower temperatures. This result is even more surprising given that the qualitative impression given by Figure 4 is that the crystalline arrays observed near the edge and the middle of the well were very similar. As stated earlier, Halperin and Nelson predicted that $0.25 \leq \eta_T \leq 0.33$ for the quasi-long-range order for the solid. We define the correlation length to be the distance beyond which $G_T(r)$ falls to below 1/e. As a result, we find that

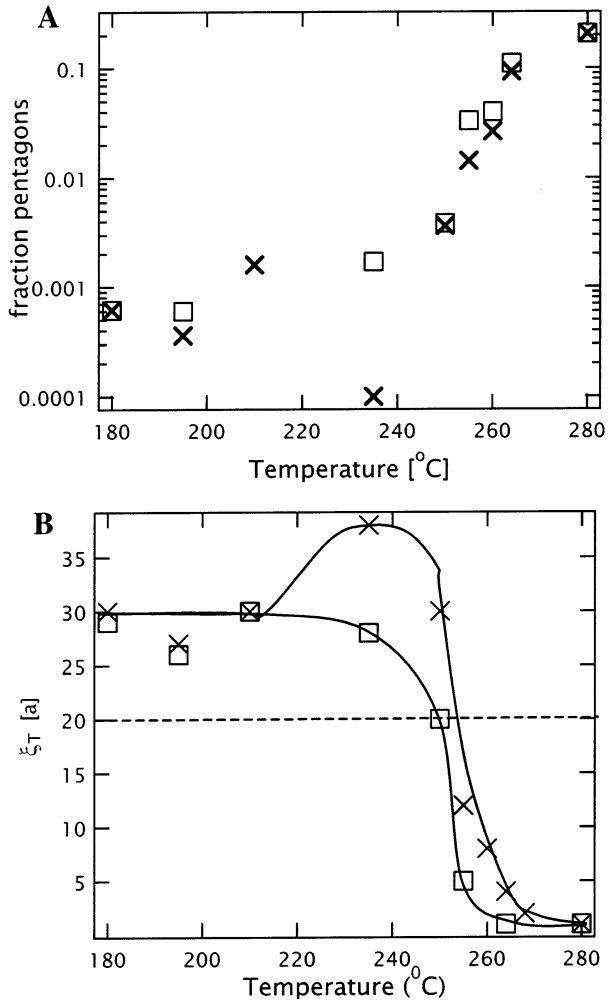


**Figure 8.** Average defect density (A) is generally lower at the edge of the 15 $\mu$m wide well (×) than in the middle (□). The translational correlation length (B) is also clearly higher at the edge of the well than in the middle. The middle of the well also passes through the dislocation pair unbinding transition ($T_m$ indicated by a dotted line at $\xi_T = 20a$) at a lower temperature than the edge.

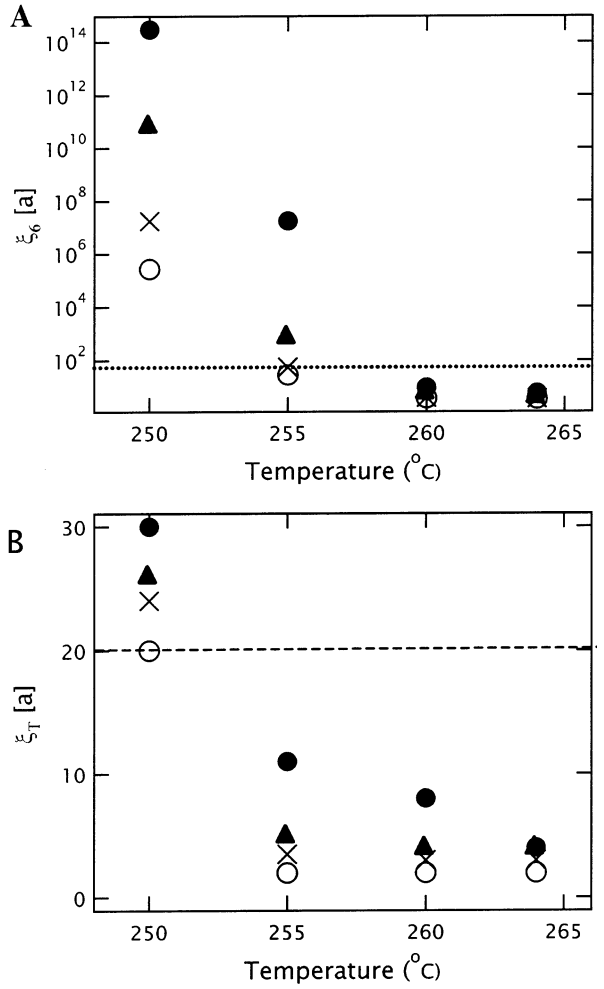


**Figure 9.** Dependence of orientational (A) and translational (B) correlation lengths on the distance from the well edge at various temperatures. Correlation lengths are calculated using 1.5 $\mu$m square areas located with center positions 0.75 (■), 2.75 (▲), 4.75 (●), and 6.75 $\mu$m (◆) from the edge. The dotted line at $\xi_T = 20a$ indicates the predicted dislocation pair unbinding transition while that at $\xi_6 = 55a$ indicates the Halperin−Nelson prediction for the disclination unbinding transition.

$\xi_T = e^{1/\eta_T}a = e^3a = 20a$ at the dislocation pair unbinding temperature, $T_m$. It is apparent from Figure 8 that $T_m$ occurs at a lower temperature away from the wall than near it.

To further analyze the effect of the edge on $T_m$ and $T_i$, the temperature of the disclination unbinding (H−N) transition, the orientational and translational correlation lengths are presented in Figure 9 as a function of temperature for a series of stripes away from the well edge. When the orientational correlation functions of the crystalline array at 250 °C were fit by an algebraic decay (eq 6), the change in $\eta_\theta$ with distance from the well edge seemed minor. When eq 7 was applied, however, it was clear that the extremely long-range orientational order of the crystalline phase near the wall at 250 °C ($\xi_6 = 10^{15}a$ where $a$ is the average lattice spacing) decays dramatically to $\xi_6 = 10^5a$ as a function of distance from the edge. Similarly, the translational correlation length at 250 °C fell by a third as the distance of the center of the 2.25 $\mu$m$^2$ area of interest to the edge was increased from 0.75 to 6.75 $\mu$m.

Halperin and Nelson's analysis of a hexatic of infinite extent on a smooth substrate led them to predict that the disclination unbinding transition will occur when the Frank elastic constant, $K_A$, drops to $(72/\pi)k_bT_i$, where $T_i$ is the temperature at the unbinding transition. At temperatures greater than $T_i$, $K_A$ is predicted drop to 0. Since the exponent $\eta_\theta$ is related to $K_A$

$$\eta_\theta = \frac{18k_bT}{\pi K_A} \tag{8}$$

$\eta_\theta$ should be 0.25 (or, through eq 7, $\xi_6 = 55a$) at the disclination unbinding transition (H−N condition). This prediction is shown in Figure 9a as a horizontal dotted line. Even though the orientational correlation length appears to be less dependent on distance from the confining edges in the hexatic and liquid regions (255−265 °C) of this semilog plot, it is significant that the H−N condition is met only at some distance away from the wall at 255 °C. It is only at this point far away from the edge at 255 °C when $\xi_6 = 55a$ that free disclinations are first observed in the SFM images.[46] The translational correlation lengths also drop continuously as a function of distance from the edge throughout this range, though the translational order is short range for both the hexatic and liquid states. Despite the fact that all the H−N conditions for the disclination unbinding

transition are met at 264 °C, Figure 7 demonstrates that some residual 6-fold symmetry still exists near the edge. The continuous drop in both translational and orientational correlation lengths with increasing distance from the edge indicates that the effect of the edge is simply to elevate $T_i$ toward the three-dimensional lattice disordering temperature ($T_{LDOT}$ = 290 °C).[35] The residual hexagonal symmetry indicates that the edge imparts orientational order onto the liquid phase just above $T_i$.

## Conclusions

The topographic edge of an underlying substrate imparts orientational and translational order to the array of block copolymer spheres. Higher translational and orientational correlation lengths are observed in all phases near the edge than away from it. In the hexatic range, the edge even serves to elevate the dislocation unbinding transition temperature ($T_m$) and the disclination unbinding transition temperature ($T_i$). The ordering effects of the edge, however, decrease continuously as the distance from the edge increases. Graphoepitaxy works to template order near the confining edge by templating particular grain orientations. The geometry of the edge, however, plays a crucial role in determining this orientation and the degree of order in its vicinity.

**Acknowledgment.** We gratefully acknowledge the financial support of the U.S. National Science Foundation DMR Polymers Program under Grant DMR 98-03738, the MRSEC Program of the National Science Foundation under Award DMR 00-80034, and the Corning Foundation for fellowship support of R.A.S. Helpful discussions with David Nelson, Glenn Fredrickson, and Sergei Magonov as well as the assistance of Tom Mates for SIMS are greatly appreciated.

## References and Notes

(1) Li, R. R.; Dapkus, P. D.; Thompson, M. E.; Jeong, W. G.; Harrison, C.; Chaikin, P. M.; Register, R. A.; Adamson, D. H. *Appl. Phys. Lett.* **2000**, *76*, 1689−1691.
(2) Guarini, K. W.; Black, C. T.; Milkove, K. R.; Sandstrom, R. L. *J. Vac. Sci. Technol. B* **2001**, *19*, 2784−2788.
(3) Black, C. T.; Guarini, K. W.; Milkove, K. R.; Baker, S. M.; Russell, T. P.; Tuominen, M. T. *Appl. Phys. Lett.* **2001**, *79*, 409−411.
(4) Cheng, J. Y.; Ross, C. A.; Chan, V. Z. H.; Thomas, E. L.; Lammertink, R. G. H.; Vancso, G. J. *Adv. Mater.* **2001**, *13*, 1174−1178, 1125.
(5) Sohn, B. H.; Seo, B. H. *Chem. Mater.* **2001**, *13*, 1752−1757.
(6) Watkins, J. J.; McCarthy, T. J. *Chem. Mater.* **1995**, *7*, 1991−1999.
(7) Kim, H. C.; Jia, X. Q.; Stafford, C. M.; Kim, D. H.; McCarthy, T. J.; Tuominen, M.; Hawker, C. J.; Russell, T. P. *Adv. Mater.* **2001**, *13*, 795−797.
(8) Thurn-Albrecht, T.; Schotter, J.; Kastle, C. A.; Emley, N.; Shibauchi, T.; Krusin-Elbaum, L.; Guarini, K.; Black, C. T.; Tuominen, M. T.; Russell, T. P. *Science* **2000**, *290*, 2126−2129.
(9) Mansky, P.; DeRouchey, J.; Russell, T. P.; Mays, J.; Pitsikalis, M.; Morkved, T.; Jaeger, H. *Macromolecules* **1998**, *31*, 4399−4401.
(10) Morkved, T. L.; Lu, M.; Urbas, A. M.; Ehrichs, E. E.; Jaeger, H. M.; Mansky, P.; Russell, T. P. *Science* **1996**, *273*, 931−933.
(11) Huang, E.; Russell, T. P.; Harrison, C.; Chaikin, P. M.; Register, R. A.; Hawker, C. J.; Mays, J. *Macromolecules* **1998**, *31*, 7641−7650.
(12) Mansky, P.; Russell, T. P.; Hawker, C. J.; Pitsikalis, M.; Mays, J. *Macromolecules* **1997**, *30*, 6810−6813.
(13) Yang, X. M.; Peters, R. D.; Nealey, P. F.; Solak, H. H.; Cerrina, F. *Macromolecules* **2000**, *33*, 9575−9582.
(14) Peters, R. D.; Yang, X. M.; Nealey, P. F. *Macromolecules* **2002**, *35*, 1822−1834.
(15) Segalman, R. A.; Yokoyama, H.; Kramer, E. J. *Adv. Mater.* **2001**, *13*, 1152−1155.
(16) Trawick, M.; Angelscu, D.; Chaikin, P. M.; Sebastian, J.; Register, R.; Adamson, D.; Harrison, C. In *Bulletin of the American Physical Society March Meeting*; Indianapolis, IN, 2002; Vol. 47, Part II, p 970.
(17) Adams, J. L.; Graessley, W. M.; Register, R. A. *Macromolecules* **1994**, *27*, 6026−6032.
(18) Adams, J. L.; Quiram, D. J.; Graessley, W. W.; Register, R. A.; Marchand, G. R. *Macromolecules* **1996**, *29*, 2929−2938.
(19) Schwab, M.; Stuhn, B. *Phys. Rev. Lett.* **1996**, *76*, 924−927.
(20) Schwab, M.; Stuhn, B. *Colloid Polym. Sci.* **1997**, *275*, 341−351.
(21) Sakamoto, N.; Hashimoto, T.; Han, C. D.; Kim, D.; Vaidya, N. Y. *Macromolecules* **1997**, *30*, 1621−1632.
(22) Sakamoto, N.; Hashimoto, T. *Macromolecules* **1998**, *31*, 8493−8502.
(23) Han, C. D.; Vaidya, N. Y.; Kim, D.; Shin, G.; Yamaguchi, D.; Hashimoto, T. *Macromolecules* **2000**, *33*, 3767−3780.
(24) Bates, F. S.; Fredrickson, G. H. *Annu. Rev. Phys. Chem.* **1990**, *41*, 525−557.
(25) Dormidontova, E. E.; Lodge, T. P. *Macromolecules* **2001**, *34*, 9143−9155.
(26) Semenov, A. N. *Macromolecules* **1989**, *22*, 2849−2851.
(27) Coulon, G.; Russell, T. P.; Deline, V. R.; Green, P. F. *Macromolecules* **1989**, *22*, 2581−2589.
(28) Russell, T. P.; Coulon, G.; Deline, V. R.; Miller, D. C. *Macromolecules* **1989**, *22*, 4600−4606.
(29) Anastasiadis, S. H.; Russell, T. P.; Satija, S. K.; Majkrzak, C. F. *Phys. Rev. Lett.* **1989**, *62*, 1852−1855.
(30) Menelle, A.; Russell, T. P.; Anastasiadis, S. H.; Satija, S. K.; Majkrzak, C. F. *Phys. Rev. Lett.* **1992**, *68*, 67−70.
(31) Yokoyama, H.; Kramer, E. J.; Rafailovich, M. H.; Sokolov, J.; Schwarz, S. A. *Macromolecules* **1998**, *31*, 8826−8830.
(32) Yokoyama, H.; Mates, T. E.; Kramer, E. J. *Macromolecules* **2000**, *33*, 1888−1898.
(33) Fredrickson, G. H. *Macromolecules* **1987**, *20*, 2535−2542.
(34) Brown, G.; Chakrabarti, A. *J. Chem. Phys.* **1994**, *101*, 3310−3317.
(35) Segalman, R. A.; Hexemer, A.; Hayward, R. C.; Kramer, E. J. *Macromolecules* **2003**, *36*, 3272−3288.
(36) Jancovici, B. *Phys. Rev. Lett.* **1967**, *19*, 20−22.
(37) Imry, Y.; Gunther, L. *Phys. Lett. A* **1969**, *A29*, 483−484.
(38) Imry, Y.; Gunther, L. *Phys. Rev. B* **1971**, *3*, 3939−3945.
(39) Mikeska, H.-J.; Schmidt, H. *J. Low Temp. Phys.* **1970**, *2*, 371−281.
(40) Mermin, N. D. *Phys. Rev.* **1968**, *176*, 250−254.
(41) Kosterlitz, J. M.; Thouless, D. J. *J. Phys., Part C: Solid State* **1972**, L124−126.
(42) Kosterlitz, J. M.; Thouless, D. J. *J. Phys., Part C: Solid State* **1973**, *6*, 1181−1203.
(43) Halperin, B. I.; Nelson, D. R. *Phys. Rev. Lett.* **1978**, *41*, 121−124.
(44) Nelson, D. R.; Halperin, B. I. *Phys. Rev. B* **1979**, *19*, 2457−2484.
(45) Young, A. P. *Phys. Rev. B* **1979**, *19*, 1855−1866.
(46) Segalman, R. A.; Hexemer, A.; Kramer, E. J. Submitted for publication.
(47) Smith, H. I.; Flanders, D. C. *Appl. Phys. Lett.* **1978**, *32*, 349−350.
(48) Berg, M. D. *Computational Geometry: Algorithms and Applications*, 2nd rev. ed.; Springer: Berlin, 2000.
(49) Segalman, R. A.; Schaefer, K.; Fredrickson, G. H.; Kramer, E. J.; Magonov, S. *Macromolecules* **2003**, *36*, 4498−4506.

MA0257696